Journal of Power Sources 196 (2011) 10359–10368

Contents lists available at ScienceDirect

Journal of Power Sources

journal homepage: www.elsevier.com/locate/jpowsour

Design optimization of electric vehicle battery cooling plates for thermal performance

Anthony Jarrett, Il Yong Kim*

Queen's University, Kingston, Ontario, K7L 3N6, Canada

ARTICLE INFO

Article history:
Received 11 May 2011
Received in revised form 23 June 2011
Accepted 24 June 2011
Available online 2 July 2011

Keywords:
Electric vehicle battery
Cooling plate
Coolant flow channel
Thermal management
Temperature uniformity
Design optimization

ABSTRACT

The performance of high-energy battery cells utilized in electric vehicles (EVs) is greatly improved by adequate temperature control. An efficient thermal management system is also desirable to avoid diverting excessive power from the primary vehicle functions. In a battery cell stack, cooling can be provided by including cooling plates: thin metal fabrications which include one or more internal channels through which a coolant is pumped. Heat is conducted from the battery cells into the cooling plate, and transported away by the coolant. The operating characteristics of the cooling plate are determined in part by the geometry of the channel; its route, width, length, etc. In this study, a serpentine-channel cooling plate is modeled parametrically and its characteristics assessed using computational fluid dynamics (CFD). Objective functions of pressure drop, average temperature, and temperature uniformity are defined and numerical optimization is carried out by allowing the channel width and position to vary. The optimization results indicate that a single design can satisfy both pressure and average temperature objectives, but at the expense of temperature uniformity.

1. Introduction

To meet the expectations of the consumer, electric vehicles (EVs) must have a performance—especially considering range and battery reliability—comparable to that of a modern combustion-engine vehicle [1,2]. One of the current limitations is in the thermal control of the battery: operation at low temperature reduces the power output due to suppressed electro-chemical reactions, while elevated temperature accelerates corrosion leading to reduced battery life [3]. It is also important that the temperature within a battery cell is uniform: variations will cause the electrochemical reactions to proceed at different rates in different regions of the cell, thereby leading to incomplete energy utilization, and inefficient management of the battery life [3]. Any power consumed for the regulation of temperature reduces the power available to the primary vehicle functions, and so the efficient operation of a thermal management system is also desirable [4].

There are some situations (e.g. starting in cold environments) for which battery heating may be required [5], but for prolonged operation cooling will certainly be required. For batteries of low energy density, it may be possible to make use of air or passive cooling, but for higher energy density batteries, an active liquid cooled system gives the most effective and efficient thermal management [6].

In order to provide enough energy, an EV battery can be expected to occupy a large volume. For the most efficient use of space, a stack of rectangular laminate battery cells is often preferred, with temperature control by cooling plates inserted between alternate cells. These are typically thin metal pressings with one or more internal channels through which a coolant is pumped. The coolant absorbs heat from the cells and carries it away to a heat exchanger external to the battery. The performance of the cooling plate (in terms of heat transfer, temperature uniformity, power consumption, etc.) is determined by the fluid–solid interactions, and by the convective heat transfer from the plate into the coolant.

Literature on the specific subject of battery cooling plates is sparse, but several studies have considered EV battery cooling in general terms, or with other battery configurations. Ghosh et al. [7] studied air-cooling of cylindrical cells using CFD, and by modifying the airflow improved the battery temperature distribution. Likewise, Kim and Pesaran [6] studied the cooling of cylindrical cells with either air, oil, or a water–ethylene glycol mix. In an indirect liquid-cooled system water–ethylene glycol is superior to oil. However, mineral oil can be used in a direct-contact cooling system in which the heat transfer coefficients are much higher.

In the thermal control of fuel cells, the objectives of mean temperature and temperature uniformity are similarly important, and thermal control can also be addressed using cooling plates. Chen

* Corresponding author. Tel.: +1 613 533 3077; fax: +1 613 533 6489.
E-mail addresses: jarretta@me.queensu.ca (A. Jarrett), iykim@me.queensu.ca (I.Y. Kim).

0378-7753/$ – see front matter.
doi:10.1016/j.jpowsour.2011.06.090

et al. [8], Choi et al. [9], and Yu et al. [10] have evaluated a number of different cooling plate designs using CFD, and found that the performance was significantly affected by the route of the cooling channel within the plate. The channel configuration can be broadly categorized into serpentine designs (a single, linear channel), parallel designs, and multi-channel designs with several inlet and outlet locations. Nam et al. [11] developed an algorithm to design different serpentine and multi-channel geometries, although as with the other studies, they were limited to uniform channel widths, and further numerical optimization was not considered.

Electronics cooling systems operate on a smaller scale than automotive applications, but have similar goals. A typical micro-channel heat sink comprises many parallel rectangular channels carrying coolant across the face of the component to be cooled. Following the work of Tuckerman and Pease [12] to characterize the system using thermal resistances, several studies have employed optimization to improve the design. Kim [13] discussed three optimization techniques: the fin method, the porous medium method and numerical optimization; the latter being considered the most accurate, but also most time consuming. Several studies have used the fin method to optimize the number of channels, thickness, and cross-section ratio [14,15]; with channel width varying along the length [16]; or with multiple layers of channels [17]. The numerical optimization method was employed by Ryu et al. [18] who found that with a constraint on pumping power, the most significant design variable was the channel width.

Kurnia et al. [19], also working in the field of microelectronics, applied the same methodology as the fuel cell studies; and with similar results. This study also introduced a mixed-objective 'figure of merit': cooling performance per unit pumping power. However, the pump power tends to be the overwhelming factor, reducing the utility of the figure of merit when cooling performance is the main concern.

Most studies of cooling channels assume square-edged channels, as these are simplest to model; however, precise manufacturing is sometimes infeasible. Fisher and Torrance [20,21] used the boundary element method to assess heat transfer into channels with rounded corners of varying degree: from rectangular through elliptical to diamond-shaped. They found that moving away from a rectangular cross-section decreases the rate of heat transfer (presumably due to a reduction in surface area), although the optimal spacing between channels becomes smaller, allowing more channels in the same space. Overall, a cooling plate with elliptical channels has heat transfer decreased by approximately 5%.

Topology optimization [22–24] has been used in the field of heat transfer and fluid flow to remove the design constraints associated with size and shape optimization. This technique divides the physical domain into elements, and each one is given a design variable to describe its state: in this case, either solid or fluid. Sensitivity analysis is then used to determine which elements should belong in either domain given a constraint on the total volume. Borrvall and Petersson [25] and Olesen et al. [26] have applied this method to find minimum power designs for fluid flow problems, which result in typical hydrodynamic geometries. Dede [27] added a second set of governing equations to solve simultaneously for energy, permitting multi-objective optimization of both pressure drop and heat transfer. Although the model does not quite represent the problem posed in this study, and its results could not be manufactured without considerable simplification, the resulting multi-scale branching structure could certainly be used as inspiration.

Evidently, thermal regulation and its associated power consumption are vital factors in the performance of an EV battery system. Although studies exist that consider the general performance and thermal characteristics of an EV battery pack, none have focused on the design of battery cooling plates. Research in the similar field of fuel cell cooling plates has used parametric studies to compare the performance of different cooling plates, indicating that the geometry is a significant factor. However, the logical conclusion of the research—a systematic optimization process—was not attempted. Conversely, studies of micro-channel heat sinks have used various optimization methods to improve their performance, but they operate on a different size scale and with different boundary conditions and constraints that prevent the results from being applied to battery cooling plates.

The objective of this paper is to apply numerical optimization to a single cooling plate in order to improve its thermal performance. Using a parameterized model generation routine, design variables controlling the cooling channel geometry are specified. Objective functions of average temperature, temperature uniformity, and power consumption (in terms of the pressure drop) are defined by CFD analysis. Numerical optimization in MATLAB is used to determine optimum cooling plate designs with respect to these three objective functions. A comprehensive verification process is applied to the CFD analysis and optimization including considerations of initial design sensitivity, and mesh independence. The study aims to reveal design principles that can be utilized in battery cooling plates, and to demonstrate that significant performance gains can be realized with optimization techniques.

2. Method

2.1. CFD model

The battery pack configuration being investigated is composed of a stack of thin rectangular battery cells. Between every pair of cells, there is a cooling plate of the same rectangular dimension. Heat from the two battery cells on either side transfers into the plate, and then into the coolant which flows through an internal channel. Each large face of the cooling plate has identical boundary conditions—heat flux from a single battery cell—and its geometry is symmetric in the thickness-wise direction. Therefore, a half cooling plate can be used in the analysis.

The cooling plate model is generated parametrically using the commercial CFD pre-processor, GAMBIT. The outer plate dimensions are 1 mm × 160 mm × 200 mm, and after applying symmetry, the modeled plate thickness reduces to 0.5 mm. The route of the cooling channel is defined by orthogonal volumes set to either the solid or fluid domain. For this study, a simplified serpentine channel configuration was selected based on the conclusions of a previous study [10] and adjusted to the proportions of the plate. This can be seen in Fig. 1.

The primary design variables in this optimization are the in-plane position and width of the coolant channel. These are controlled by parameterizing the x and y dimensions of the construct volumes while keeping all construction lines orthogonal; the parameterization of the geometric design variables is shown in Fig. 2. Some possible variations on the cooling channel geometry are shown in Fig. 3.

243,560 hexahedral elements are used to construct the mesh; of which 231,336 are in the fluid domain. Boundary layers are used in the fluid to increase the mesh density close to the wall in order to resolve heat transfer phenomena.

2.2. CFD analysis

Analysis of the cooling plate is carried out in the commercial CFD solver, FLUENT. After importing the model, boundary conditions of symmetry, mass flow inlet, pressure outlet and heat generation are applied. In this study, the coolant mass flow rate is kept constant at 1×10^{-3} kg s^{-1} at a uniform inlet temperature of 300 K (after

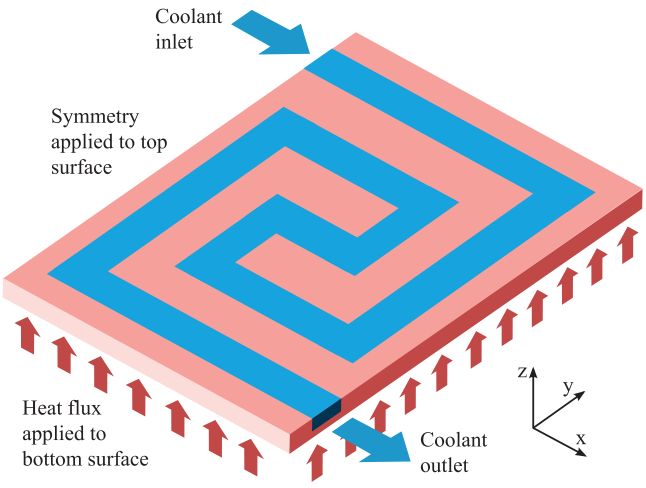

Fig. 1. Schematic of CFD analysis model.

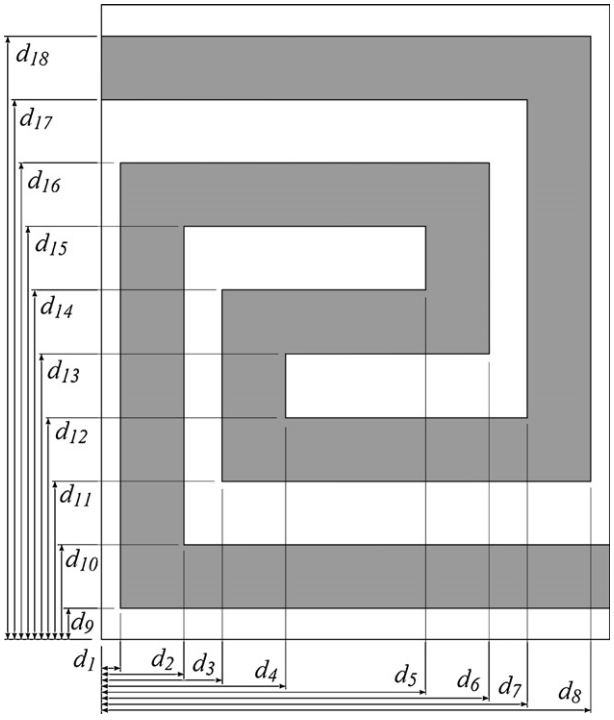

Fig. 2. Description of cooling plate channel by 18 design variables. The channel is indicated in gray.

accounting for the symmetry condition, 5×10^{-4} kg s^{-1} is applied). A uniform heat flux of 500 W m^{-2} is applied through the large bottom face of the cooling plate, as shown in Fig. 1. Material properties

Table 1
Cooling plate analysis parameters.

Material properties	Value
Coolant fluid	Water–ethylene glycol
Coolant viscosity[a] (Pa s)	0.00315
Coolant conductivity (W m^{-1} K^{-1})	0.419
Coolant specific heat[a] (J kg^{-1} K^{-1})	3494
Coolant density (kg m^{-3})	1065
Plate material	Aluminum
Plate conductivity (W m^{-1} K^{-1})	202
Plate specific heat (J kg^{-1} K^{-1})	871
Plate density (kg m^{-3})	2719
Dimensions	
Plate thickness (mm)	1
Plate width (mm)	160
Plate height (mm)	200
Channel thickness (mm)	0.75
Initial channel width (mm)	20
Boundary Conditions	
Coolant inlet mass flow (kg s^{-1})	0.001
Coolant inlet temperature (K)	300
Coolant outlet pressure (Pa)	0
Heat flux (W m^{-2})	500

[a] Property stated at 300 K.

of aluminum and a water–ethylene glycol mix are applied to the plate and coolant respectively. A list of analysis parameters is given in Table 1; plate dimensions and boundary conditions are based on data supplied by our industrial partner, General Motors of Canada.

Note that during the optimization process, the channel width varies, thereby changing the inlet fluid velocity. A fixed mass flow rate was selected over the alternatives of fixed velocity or pressure in order to maintain the thermal balance associated with the fluid inputs and outputs. At these fluid conditions, the Reynolds number of the reference design (uniform channel width of 20 mm) is 30.6. The characteristic length for the calculation of the Reynolds number is the hydraulic diameter, which is equal to four times the cross-sectional area of the channel divided by the wetted perimeter. During optimization the Reynolds number changes because the channel dimensions vary: it can have a value between approximately 16 (channel width of 40 mm), and 231 (channel width of 2 mm).

The FLUENT CFD solver is used to solve the governing equations for the conservation of mass, momentum and energy for a Newtonian incompressible fluid. This study only considers the steady state condition, and the relevant equations are summarized as

$$\frac{\partial u_j}{\partial x_j} = 0$$

$$\rho u_j \frac{\partial u_i}{\partial x_j} + \frac{\partial p}{\partial x_i} = \mu \Delta u_i$$

$$\rho c u_j \frac{\partial T}{\partial x_j} = \frac{\partial}{\partial x_j}\left(k \frac{\partial T}{\partial x_j}\right)$$

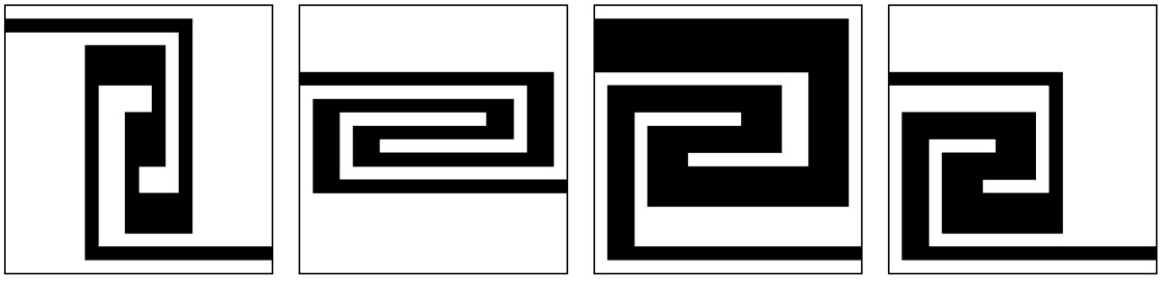

Fig. 3. Variations in design variables of cooling plate geometry: black areas indicate the cooling channel; coolant flow is from top-left to bottom right.

where u and x represent the velocity and direction vectors in Cartesian space; ρ is the density; p is the pressure; μ is the fluid viscosity; c is the specific heat capacity; T is the temperature; k is the thermal conductivity; Δ is the Laplacian operator.

For the coupling of the continuity and momentum equations, the SIMPLE algorithm was used with second- and third-order equations (high order analysis options were used for more stable output—vital for optimization finite differencing). The solution was terminated when the residuals of the x- and y-velocity equations reduced below 10^{-7}; testing confirmed that at this point, all residuals were smaller than 5×10^{-6} and the output parameters were converged.

Following the completion of the analysis, the key performance objectives are reported and output to text files: mean temperature on the heat flux surface; standard deviation of temperature on the same surface; and total pressure on the inlet and outlet surfaces. Note that with a constant heat flux and coolant temperature, the mean plate temperature is a good indicator of heat transfer efficiency: i.e. the smallest temperature gradient between the plate and coolant that will drive the applied heat flux. In addition, note that at a constant mass flow rate, the total pressure drop can be used as a proxy for power consumption.

2.3. Optimization

The optimization statement can be expressed formally as follows:

$$\begin{aligned}
&\text{minimize} && : \quad P_{\text{fluid}}(\boldsymbol{d}) \\
&&& \quad\;\; T_{\text{avg}}(\boldsymbol{d}) \\
&&& \quad\;\; T_{\sigma}(\boldsymbol{d}) \\
&\text{subject to} && : \quad t_{\text{wall}}(\boldsymbol{d}) \geq \Delta \\
&\text{where} && : \quad P_{\text{fluid}} = P_{\text{inlet}} - P_{\text{outlet}} \\
&&& \quad\;\; T_{\text{avg}} = \frac{\int_{A_0} T dA}{\int_{A_0} dA} \\
&&& \quad\;\; T_{\sigma} = \sqrt{\frac{\int_{A_0} (T - T_{\text{avg}})^2 dA}{\int_{A_0} dA}}
\end{aligned}$$

where P_{inlet} and P_{outlet} are the area weighted average total pressure on the inlet and outlet faces respectively; T_{avg} and T_{σ} are the mean and standard deviation of the temperature defined over the bottom surface of the plate, A_0. The design variable vector, $\boldsymbol{d}$, holds the 18

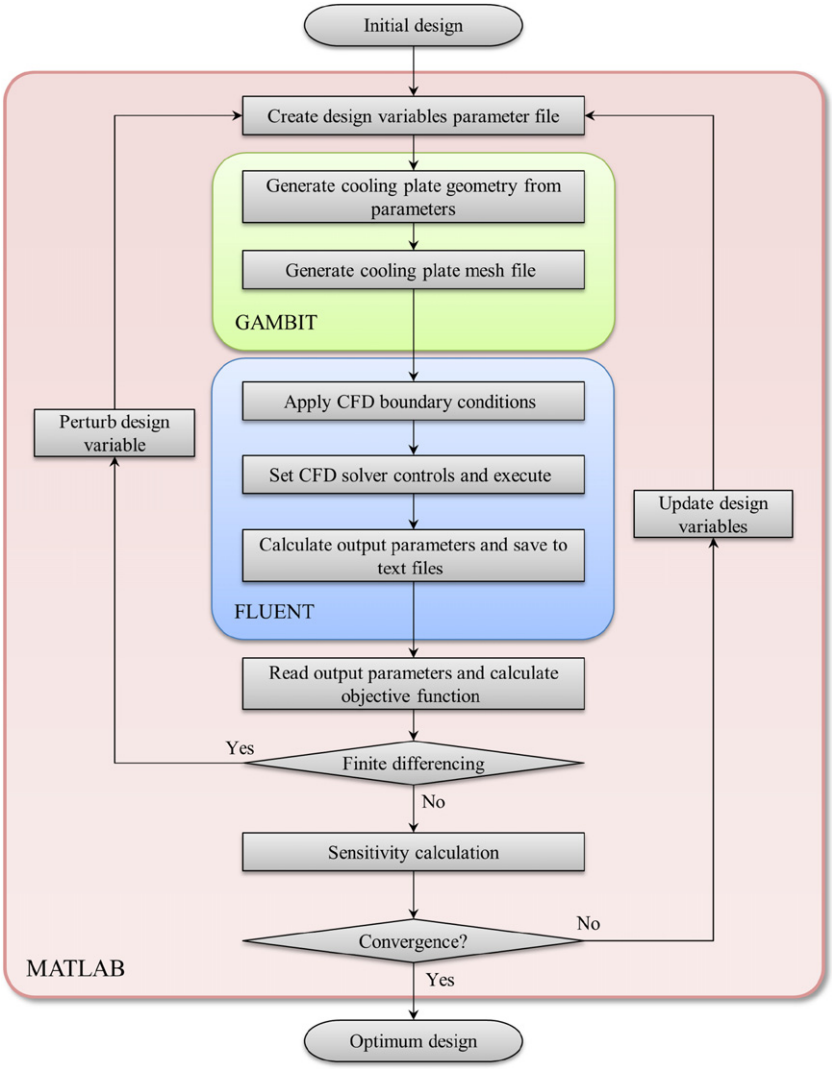

Fig. 4. Flowchart describing the optimization process.

dimensions needed to describe the shape of the cooling channel in the x–y plane. The constraint function, t_{wall}, is the minimum solid or fluid section thickness. This is constrained to be always greater than Δ; 2 mm in this case.

These parameters comprise a non-linear constrained optimization problem. A routine has been written in the MATLAB programming environment utilizing the inbuilt sequential quadratic programming algorithm, 'fmincon' to derive a solution. First a design vector corresponding to a cooling plate geometry is passed to GAMBIT, which generates the model and meshes it. MATLAB calls FLUENT, which runs the CFD analysis and returns the output parameters to MATLAB. This constitutes a single objective function evaluation. The MATLAB optimization function makes use of a finite differencing algorithm and multiple objective function evaluations to calculate the design sensitivity with respect to the desired objective function. This is used to update the design variables, and another design iteration begins. A convergence criterion based on objective function change is used to terminate the optimization at the appropriate time. This process is described in Fig. 4 by a flowchart.

2.4. Model verification

There are several aspects of the optimization process to which verification measures can be applied: the absolute accuracy of the CFD analysis, the objective function accuracy, the optimization algorithm, and the converged cooling plate design. The two that have the greatest influence are the objective function accuracy, and the optimization algorithm; confidence in the optimization result is significantly increased if these two factors can be verified.

The termination of a CFD analysis is controlled by specifying limits on the calculation residuals. In this case, ideally, the analysis should stop as soon as the objective functions have reached a steady converged value. To translate this requirement to a residual-based convergence criterion, three different cooling plate designs were assessed to identify the point at which all objective functions had converged. It was found that objective function convergence could reliably be obtained with limits of 10^{-7} on the x- and y-velocities. An additional solver verification step is to check that the thermal imbalance within the CFD analysis is negligible; assessment of the converged model has confirmed that the net imbalance is typically smaller than 10^{-6}% of the total heat flow.

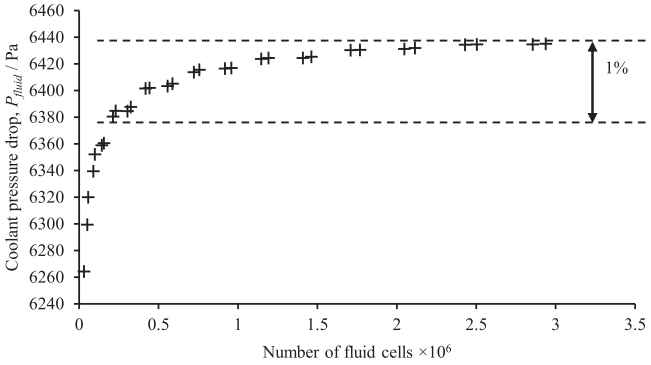

Fig. 5. Mesh convergence plot of pressure drop (P_{fluid}) objective function.

The accuracy of a CFD analysis generally increases as the number of elements is increased. However, computing expense should also be considered, especially for optimization which requires hundreds of function evaluations (CFD analyses). Therefore, a mesh convergence study was performed to establish a mesh size that would give adequate results at an acceptable computing time. Meshes of between 30,000 and 3,000,000 elements were generated and the three objective functions were monitored during the mesh convergence test. The T_{avg} and T_{σ} outputs showed variations of less than 1% across the entire tested range. The P_{fluid} convergence plot is shown in Fig. 5 with a 1% band marked, which indicates that a mesh of approximately 250,000 elements is required to be within 1% of the converged value. Repeating the test with several different plate designs confirmed that with a mesh of 243,560 elements, all three objective functions are within 1% of their converged value. Therefore all optimization was carried out using a mesh of this size.

In order to reduce the risk that the optimization converges on a local minimum, the optimizations of T_{avg} and T_{σ} were performed from eight different initial designs. To choose a well-distributed set of designs, Latin hypercube sampling (LHS) [28] was used. This

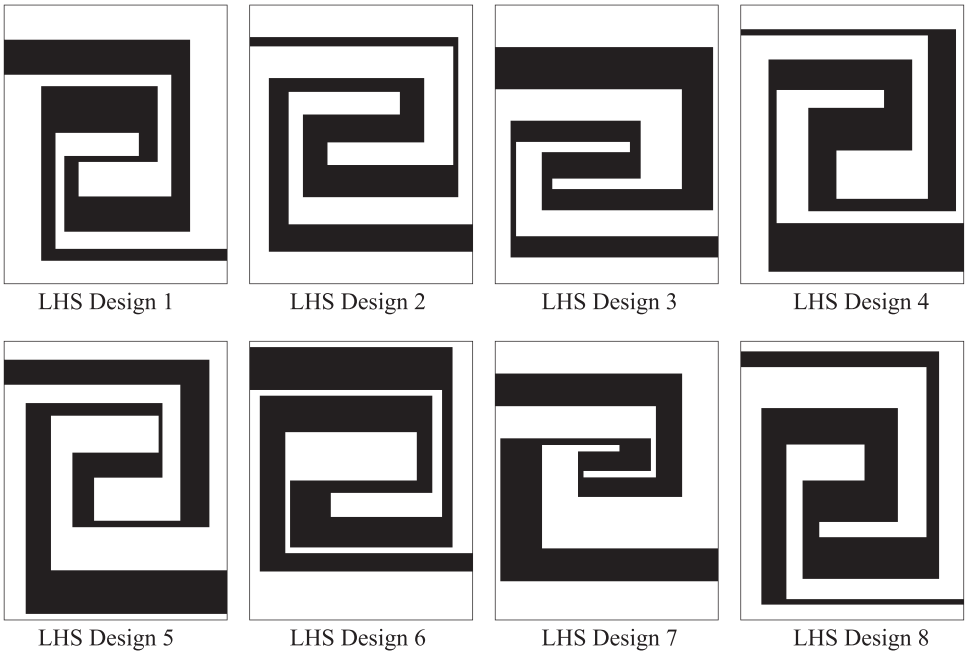

Fig. 6. Set of initial cooling channel designs selected using Latin hypercube sampling.

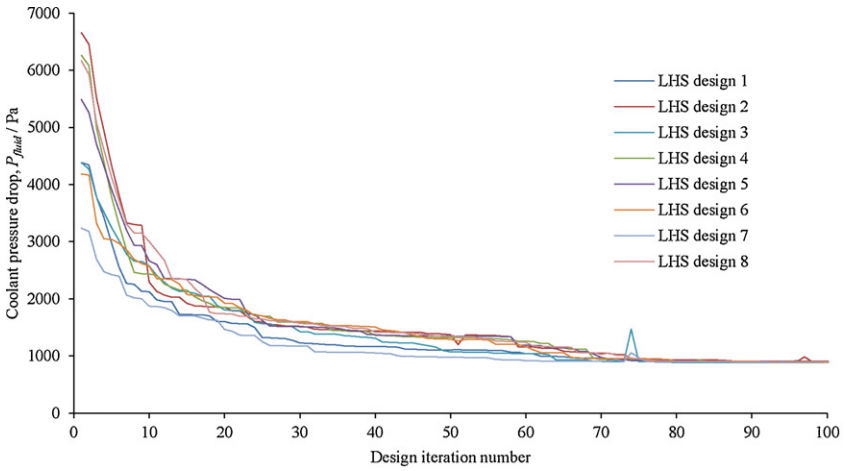

(a) P_{fluid} convergence

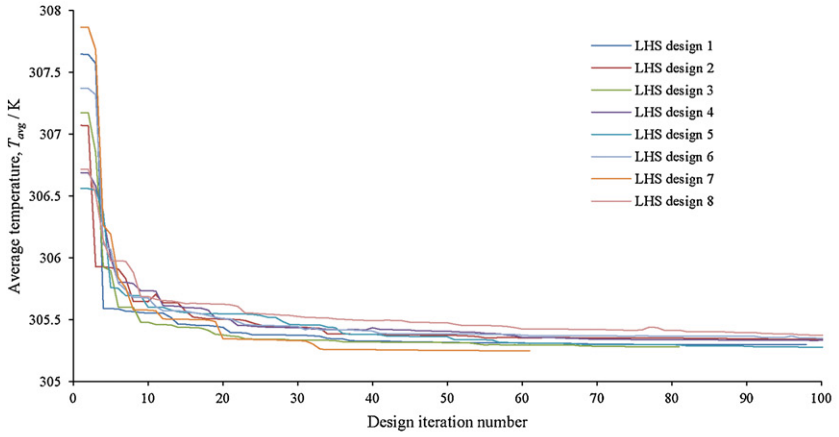

(b) T_{avg} convergence

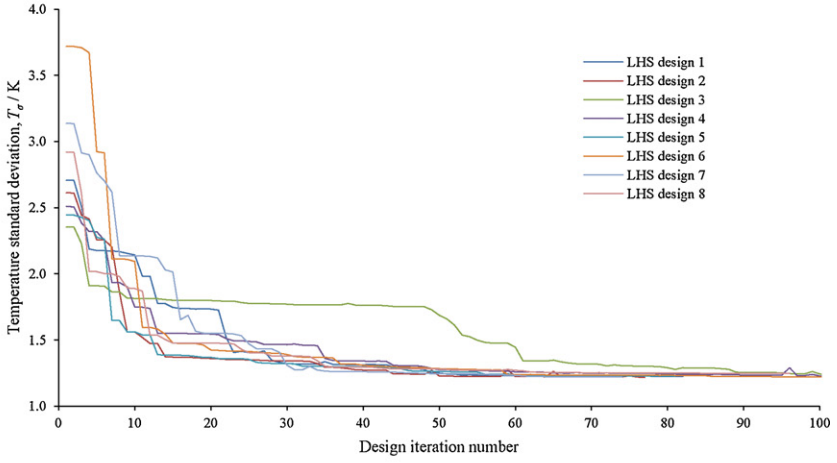

(c) T_σ convergence

Fig. 7. For every objective function, eight optimizations were performed from different initial designs. These charts show the convergence of the objective function over the optimization duration.

ensures that every design variable is represented at a range of values. The eight initial designs are shown in Fig. 6.

Due to variation in the channel geometry, the Reynolds number of the coolant flow can vary between approximately 15 and 230. In an ideal rectangular conduit the transition from laminar to turbulent flow occurs at a Reynolds number between 1900 and 2800, depending on the aspect ratio [29]. However, the channel corners and changes in cross-section have the potential to reduce the transition point. Flow around a square-edged U-bend of a fuel cell cooling plate was studied by Martin et al. [30] at Reynolds

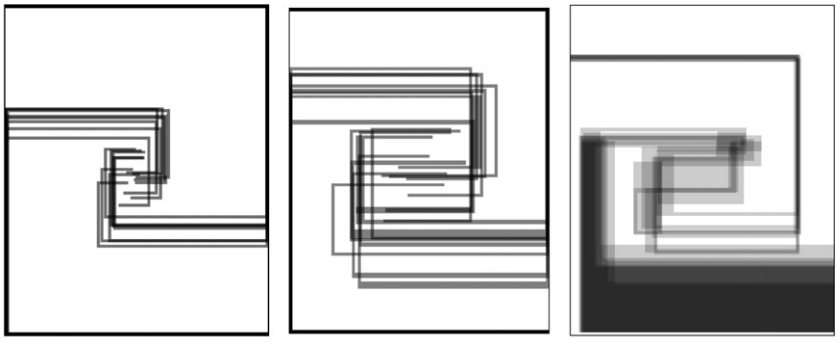

(a) P_{fluid} optimized designs (b) T_{avg} optimized designs (c) T_{σ} optimized designs

Fig. 8. Superimposed geometry of the optimized designs produced from eight initial designs. For clarity, the T_{avg} and P_{fluid} designs are shown with the cooling channel in white, and the T_{σ} designs with the cooling channel in black.

numbers between 109 and 872. Up to a Reynolds number of 436 the flow was laminar and steady, but above this, the flow became time-dependent: the precursor of turbulent flow. Although this suggests that in the present study a laminar analysis will be accurate, some caution must be applied: the channel aspect ratio is quite different, and the proximity of consecutive bends may modify the Reynolds number and influence the onset of instability. Nonetheless, it provides some confidence that an assumption of laminar flow is reasonable at the conditions used in this study.

3. Results and discussion

3.1. Optimization convergence

The optimization routine was run for each of the three objective functions using the algorithm and settings described above. The optimizations ran until the change in objective function between iterations reduced to below 0.0001% (up to a limit of 100 iterations). Such a small convergence criterion was used to prevent premature termination: there were frequently design iterations with negligible objective function change followed by further improvement.

The Latin hypercube sample of eight initial designs was used for the optimizations of all three objective functions. The reduction in objective function during the optimizations is shown in Fig. 7: the eight lines on each chart correspond to the eight optimizations. In each case there is a rapid decrease in the first 15–20 design iterations, and by iteration 30 the objective function is typically quite close to the final value. However, there is one optimization of T_{σ} (initial design 3) that stands out: even by iteration 50, it is still more than 40% from the final value. However, by iteration 100, the objective functions of all designs are within a narrow range. The T_{avg} converged designs lie within a 2.5% band, while the T_{σ} and P_{fluid} converged designs have less than 1% scatter.

Although the optimization of the eight LHS initial designs produce almost equivalent objective function values, their converged designs are in some cases quite different from each other, and this indicates that in the design space there are many local minima present with almost equivalent performance. To visualize the similarities and differences between the converged designs, Fig. 8 shows the geometry of all eight cooling channels superimposed, and with some translucency applied. The T_{avg} optimized cooling channel displays significant variation in all regions of the plate: there are almost no two designs in which a channel section is in the same position. The P_{fluid} optimized cooling channel is similar, but with less spread in channel location. The feature common to all T_{avg} and P_{fluid} designs is that the cooling channel occupies the largest area possible. The T_{σ} optimized cooling channel has two channel sections that are near identical in all eight designs; these are the two closest to the inlet. The rest of the channel has significant variation in location and width.

In the following discussions, the results presented refer to those optimizations that achieved the lowest objective function.

3.2. Optimum cooling plate characteristics

In addition to the three optimizations, the reference design was assessed for the purpose of benchmarking. Table 2 shows the output parameters of the three optimized cooling plates in addition to the reference design. The T_{avg} optimization decreased the average temperature by about 14% compared to the reference (considering the elevation above the coolant inlet temperature); the P_{fluid} and T_{σ} optimizations both showed improvements of greater than 50% in their respective objective functions.

The geometry of the four designs is shown in Fig. 9, and Table 3 lists the corresponding design variable magnitudes. This demonstrates that the optimum channel geometries for the T_{avg} and P_{fluid}

Table 2
Objective function values of optimized cooling plates compared with the reference design.

Geometry	P_{fluid} (Pa)	T_{avg} (K)	T_{σ} (K)
Reference	2948	306.09	2.64
P_{fluid} optimized	911	305.29	2.53
T_{avg} optimized	1232	305.25	2.32
T_{σ} optimized	25,124	308.31	1.22

Table 3
Value of the design variables in the reference design, and the three optimum designs.

Design Variable	Dimension (mm)			
	Reference	P_{fluid} optimized	T_{avg} optimized	T_{σ} optimized
d_1	6	2.0	2.0	7.2
d_2	26	62.8	41.1	16.0
d_3	38	64.8	46.6	49.8
d_4	58	76.2	67.0	55.7
d_5	102	82.2	88.4	96.6
d_6	122	93.5	112.0	111.3
d_7	134	95.5	118.6	135.4
d_8	154	158.0	158.0	137.4
d_9	10	2.0	2.0	2.0
d_{10}	30	56.4	67.2	42.8
d_{11}	50	58.4	70.2	59.1
d_{12}	70	82.2	101.0	61.1
d_{13}	90	84.2	103.0	105.7
d_{14}	110	96.2	119.7	108.0
d_{15}	130	98.2	121.9	116.9
d_{16}	150	124.0	144.6	118.9
d_{17}	170	126.0	146.6	167.7
d_{18}	190	198.0	198.0	169.7

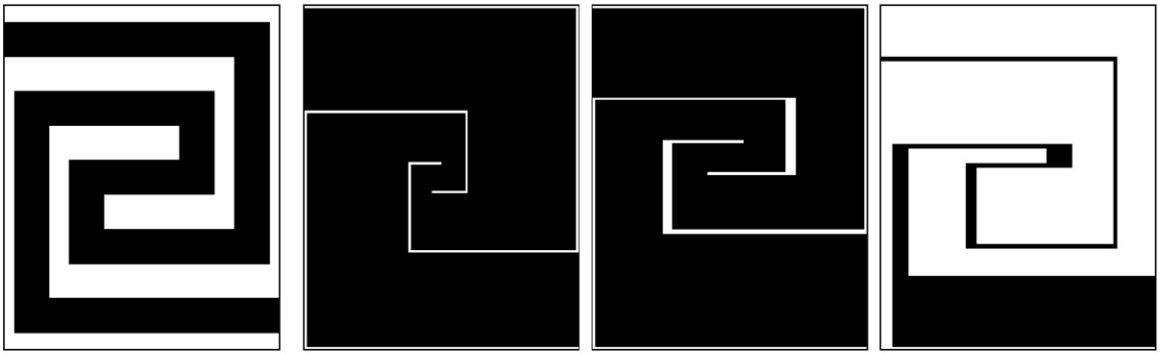

Fig. 9. Cooling plate geometry of reference design and optimized designs. The cooling channel is shown in black.

objective functions are very similar: in both cases the cooling channel occupies nearly the maximum possible area, although there is some variation in the channel geometry in the centre of the plate. Conversely, the T_σ optimized channel is close to the minimum possible width for most of its length; only widening at the last channel section. The P_{fluid} optimized design is interesting in that the cooling channel does not have uniformly wide channels: the flow area near the edge of the plate is increased at the expense of having a narrow orifice at the centre of the plate.

The total surface area of the channel was calculated for each model to better understand the heat transfer relationships; they are as follows:

Reference	0.38 m^2
P_{fluid} optimized	0.061 m^2
T_{avg} optimized	0.060 m^2
T_σ optimized	0.018 m^2

Both the P_{fluid} and T_{avg} optimized designs have approximately 50% greater channel surface area than the reference design; the area of the T_σ optimized plate has decreased by approximately 50%. These changes in channel surface area broadly correspond to the relative average temperatures of the cooling plates.

Fig. 10 shows the temperature distribution on the back face of the four cooling plate designs. As shown in Fig. 11, the temperature on the symmetry plane is almost identical. From Fig. 10a— the temperature distribution of the reference design—the effect of the coolant can clearly be seen: it enters the plate from the top left corner, where it exerts a large cooling force. As it passes through the plate, it absorbs heat, raising its temperature and reducing the cooling effect. It exits the plate at the bottom right at a temperature approximately 9K higher than the inlet temperature. This results in a general temperature gradient in the plate from top to bottom.

That the T_{avg} optimized design has a channel that is as wide as possible indicates that at these boundary conditions, a greater surface area leads to more effective total heat transfer (even though the coolant velocity is lower in a wider channel). However, note that the P_{fluid} optimized design actually has slightly greater channel surface area, but less effective heat transfer: obviously surface area is not the only factor in determining heat transfer.

Considering the geometry of the T_σ design illustrates the converse of this: that a narrow channel of fast flowing coolant reduces the total heat transfer. The temperature gradient decreases along the length of the channel, so in order to produce a uniform temperature distribution, the heat transfer into the channel must become more effective to compensate. The T_σ optimization has produced a design that starts with a very thin channel, and increases towards the outlet; therefore confirming that at constant volumetric flow, the most significant factor affecting heat transfer is the channel width.

Further investigation of the heat transfer is provided by examining the temperature profiles within the coolant and plate in the through-thickness direction. For the T_σ optimized design, the temperature profiles have been assessed in three locations: near the inlet, in the centre of the plate, and near the outlet; shown in Fig. 12. This demonstrates the increasing temperature of the coolant and plate from inlet to outlet, and the corresponding decrease in temperature gradient (and therefore local heat transfer) through the channel. The first two profiles correspond to narrow channel sections, while the third is in a wide channel section with lower fluid velocity. The temperature gradients in these profiles show that the local rate of heat transfer is higher in a narrow channel, but as demonstrated by the T_{avg} design, greater surface area leads to more effective heat transfer overall.

3.3. Limitations and further work

The primary limitation of this study is the restricted design space that the optimization operates within. Regardless of the design of the true optimum cooling plate, this optimization routine is unable to modify the cooling plate topology (e.g., the number of channels), and so can only investigate local optima that lie in this design domain. Although a different topology can be used, the choice is made by the operator and optimization would still be restricted to that design space. In order to introduce greater design freedom, a different optimization algorithm would be required—possibly akin to the topology optimization described in the introduction, or a genetic algorithm. A particular feature of the selected geometry is the sharp 90° corners; these are used to provide a consistent meshing scheme. These generate a pressure loss which is presumably sub-optimal and in any case manufacturing sharp corners is often infeasible. In addition, the corners reduce the speed of the CFD solver and lead to unnecessarily long solution times.

The boundary conditions have also been restricted to a single set of conditions in order to focus on the optimization method. However, during electric vehicle operation, a cooling plate would experience a wide range of conditions, and a thorough optimization would consider whether the design is an optimum at all conditions. Furthermore, it has been shown [31] that battery cells generate heat with a non-uniform distribution; this may influence the outcome of the design optimization. The assessment of the thermal objective functions on the face of the cooling plate is also a simplification, as the battery cell is the real target for thermal optimization; therefore, the model should be expanded to analyze conduction between the battery cell and cooling plate.

Several assessments have addressed the analysis and optimization accuracy; however, there is still scope for further work to

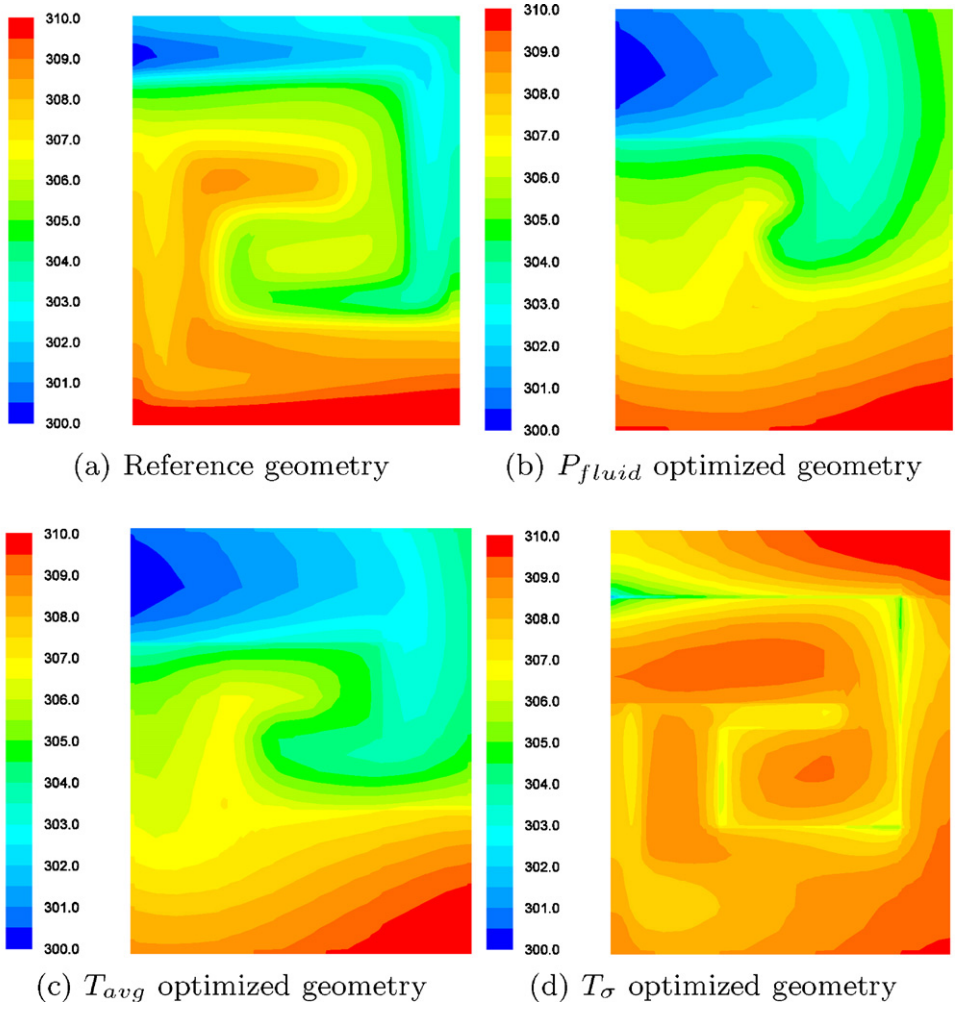

Fig. 10. Temperature distributions on the back face of reference and optimized cooling plate designs.

improve on these. At higher coolant flow rates, a consideration of unsteady or turbulent flow will be required, although it might be preferable to limit investigation to laminar regimes. A more thorough study of optimization convergence may find settings that can reduce the iterations required, or more precisely locate the global optimum.

Of the three objective functions investigated, it has been found that two are closely aligned, and produce a similar optimized design, and the third is significantly different. However, single objective optimization provides no information about intermediate designs; for example, the trade-off required in one objective to realize an improvement in the other. For this, a multi-objective

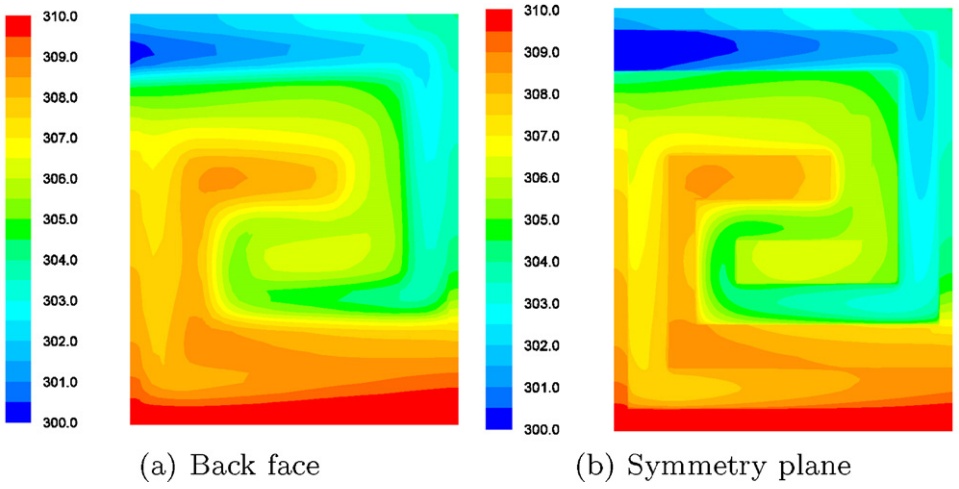

Fig. 11. Comparison of reference design temperature distributions on the back face and symmetry plane of the cooling plate. The symmetry plane shows the temperature of both solid and fluid regions.

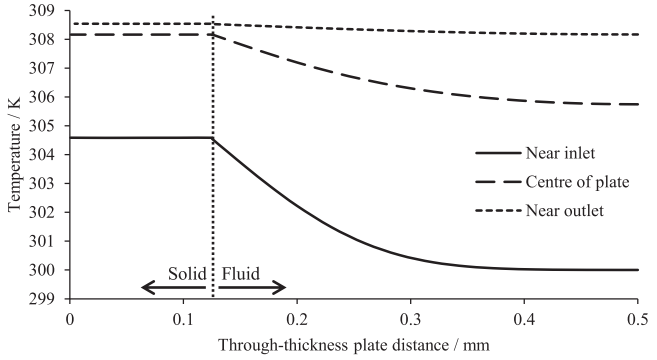

Fig. 12. Temperature profiles in the through-thickness (z) direction, sampled at three positions of the T_σ optimized plate. The sampling path was at the centre of the channel, and extends the full thickness from the heat flux boundary face to the symmetry face.

optimization study would be required, and this will be one of the goals of further research.

4. Conclusions

A process for the thermal optimization of cooling plates has been defined and assessed using the example of a plate with 18 geometric design variables. Using a numerical optimization algorithm incorporating a CFD analysis, optimum designs have been determined with respect to objective functions of coolant pressure drop, temperature uniformity, and average temperature. It was found that the optimum design for lowest average temperature is almost identical to that for lowest pressure drop; i.e. channels of the greatest possible width. The design for temperature uniformity has a narrow inlet channel widening towards the outlet; this balances the effects of coolant velocity, heat transfer area, and fluid–solid temperature gradient to equalize the heat transfer from all areas of the plate.

The convergence behaviour was investigated through a study of eight initial designs, which showed the speed of convergence could vary by up to a factor of two depending on the initial design. In the optimizations of both temperature uniformity and average temperature, the converged objective functions were almost identical but aspects of the design geometry varied significantly. This indicates many local optima with equivalent performance.

The principal limitations of the study have been the limited design space explored, and restricted boundary conditions. Future work will investigate the performance and optimum designs at different boundary conditions, non-uniform heat generation, and expand the design space to consider other cooling channel geometries.

Acknowledgments

This research is funded by AUTO21, a member of the Network of Centres of Excellence of Canada program. Technical advice and direction was gratefully received from Derrick Chow, Brian Tossan, Justin Gammage, Carlton Fuerst, and colleagues at GM Canada.

References

[1] B.K. Sovacool, R.F. Hirsh, Energy Policy 37 (3) (2009) 1095–1103.
[2] D. Bunch, M. Bradley, T. Golob, R. Kitamura, G. Occhiuzzo, Transport. Res. Part A: Policy Pract. 27 (3) (1993) 237–253.
[3] A.A. Pesaran, A. Vlahinos, S.D. Burch, Proceedings of the 14th International Electric Vehicle Symposium, Orlando, Florida, December 15–17, 1997.
[4] A.A. Pesaran, S.D. Burch, M. Keyser, Proceedings of the 4th Vehicle Thermal Management Systems Conference and Exhibition, 1999, pp. 24–27.
[5] A.A. Pesaran, A. Vlahinos, T. Stuart, 6th ASME-JSME Thermal Engineering Joint Conference Proceedings, Hawaii Island, Hawaii, 2003.
[6] G.H. Kim, A.A. Pesaran, 22nd International Battery, Hybrid and Fuel Cell Electric Vehicle Conference and Exhibition, Yokohama, Japan, 2006.
[7] D. Ghosh, P.D. Maguire, D.X. Zhu, Design and CFD simulation of a battery module for a hybrid electric vehicle battery pack, Tech. Rep. 2009-01-1386, SAE, 2009.
[8] F.C. Chen, Z. Gao, R.O. Loutfy, M. Hecht, Fuel Cells 3 (4) (2003) 181–188.
[9] J. Choi, Y.H. Kim, Y. Lee, K.J. Lee, Y. Kim, J. Mech. Sci. Technol. 22 (7) (2008) 1417–1425.
[10] S.H. Yu, S. Sohn, J.H. Nam, C.J. Kim, J. Power Sources 194 (2) (2009) 697–703.
[11] J.H. Nam, K.J. Lee, S. Sohn, C.J. Kim, J. Power Sources 188 (1) (2009) 14–23.
[12] D.B. Tuckerman, R.F.W. Pease, IEEE Electron Device Lett. 2 (5) (1981) 126–129.
[13] S.J. Kim, Heat Transfer Eng. 25 (1) (2004) 37–49.
[14] R.W. Knight, J.S. Goodling, D.J. Hall, J. Electron. Packag. 113 (3) (1991) 313–321.
[15] R.W. Knight, D.J. Hall, J.S. Goodling, R.C. Jaeger, IEEE Trans. Compon. Hybrid Manuf. Technol. 15 (5) (1992) 832–842.
[16] H.H. Bau, Int. J. Heat. Mass Transfer 41 (18) (1998) 2717–2723.
[17] X. Wei, Y. Joshi, IEEE Trans. Compon. Packag. Technol. 26 (1) (2003) 55–61.
[18] J.H. Ryu, D.H. Choi, S.J. Kim, Int. J. Heat Mass Transfer 45 (13) (2002) 2823–2827.
[19] J.C. Kurnia, A.P. Sasmito, A.S. Mujumdar, Appl. Therm. Eng. 31 (2011) 1293–1304.
[20] T.S. Fisher, K.E. Torrance, Int. J. Heat Mass Transfer 43 (1) (2000) 113–126.
[21] T.S. Fisher, K.E. Torrance, IEEE Trans. Adv. Packag. 24 (4) (2001) 555–562.
[22] M.P. Bendsøe, O. Sigmund, Topology Optimization: Theory, Methods and Applications, Springer Verlag, 2003, ISBN 3540429921.
[23] I.Y. Kim, B.M. Kwak, Int. J. Numer. Methods Eng. 53 (2002) 1979–2002.
[24] I.Y. Kim, O. Weck, Struct. Multi. Optim. 29 (6) (2005) 445–456.
[25] T. Borrvall, J. Petersson, Int. J. Numer. Methods Fluids 41 (1) (2003) 77–107.
[26] L.H. Olesen, F. Okkels, H. Bruus, Int. J. Numer. Methods Eng. 65 (7) (2006) 975–1001.
[27] E.M. Dede, Proceedings of the COMSOL User Conference, Boston, MA, 2009.
[28] M.D. McKay, R.J. Beckman, W.J. Conover, Technometrics 21 (2) (1979) 239–245.
[29] R.W. Hanks, H.C. Ruo, Ind. Eng. Chem. Fundam. 5 (4) (1966) 558–561.
[30] J. Martin, P. Oshkai, N. Djilali, J. Fuel Cell Sci. Technol. 2 (2005) 70–80.
[31] U.S. Kim, C.B. Shin, C.S. Kim, J. Power Sources 189 (1) (2009) 841–846.